SIMULATION OF ELASTIC PROPERTIES OF SPACER FABRICS AND ITS EFFECTIVE PERMEABILITY AT DIFFERENT COMPRESSION STATES

A. Fassbender[1], J. Orlik[1], K. Pietsch[2], S. Rief[1*] and A. Shamanskiy[1]

[1]ITWM Fraunhofer
Fraunhofer-Platz 1, 67663 Kaiserslautern, GERMANY
Email: fassbend@itwm.fhg.de, orlik@itwm.fhg.de,
stefan.rief@itwm.fhg.de, shamanskiy@itwm.fhg.de

[2]Institute of Textile Machinery and High Performance Material Technology
Technical University Dresden, GERMANY
Email: kathrin.pietsch@tu-dresden.de

ABSTRACT

We consider spacer fabrics, who are plates or shells composed of two knitted plane layers connected by vertical beams. Several small parameters occur in the structure, the period, the thickness of the fibers and the height of the spacer fabric. Our aim is to compute the effective stiffness and permeability of such spacer fabrics. In order to reduce the computational effort and simplify the computational model, homogenization and dimension reduction techniques are applied to replace the fabric by an equivalent two-dimensional plate or shell with effective elastic properties and simultaneously to keep the resolved micro-structure for the fluid simulation, to compute its effective permeability. The corresponding analysis for the scale separation and the detailed description of the algorithm can be found in [7]. The relation between the small parameters and the kind of the loading determine the dominance of the bending or tension of beams on the micro-level. This paper demonstrates the algorithm on an application example. We compute the elastic properties of a spacer fabric and its effective permeability for different stages of the compression of the spacer fabric. Numerical examples were performed by the successive application of the multi-scale simulation tools, Fiber FEM and GeoDict, developed at Fraunhofer ITWM and compared with the corresponding experimental results, based on measurements performed at the TU Dresden.

1   PREPROCESSING. STUDY OF THE GEOMETRY

The spacer fabrics considered in this article are based on work by Helbig [5], where the precise description can be found. The real physical samples were provided by company ESSEDEA and TU Dresden. They consist of two thick horizontal layers interconnected by knitting of thin threads (called *monofiles*), forming a 3D-structure (see Figure 1). Several types of material are available. Each is parameterized by the distance between the layers, *dist*, the number of columns the monofile crosses when going diagonally between the layers, *diag* and the radius of the monofile threads *radius*. Two provided samples were of thickness 20mm and 50mm. Both were analysed carefully in order to understand the inner structure of the material. A basic knitting pattern can be understood from Figure 2, where a magnified 3D model is presented. A combination of these basic elements forms rows and columns of the entire material. Its structure is presented in more details in Figure 3. Although only two types of material were available, at the modelling stage, eight different types were simulated using different parameters, in order to understand better the dependencies between the geometry and effective elastic and permeable properties. Two real physical samples are referred to as Samples 4 and 8.
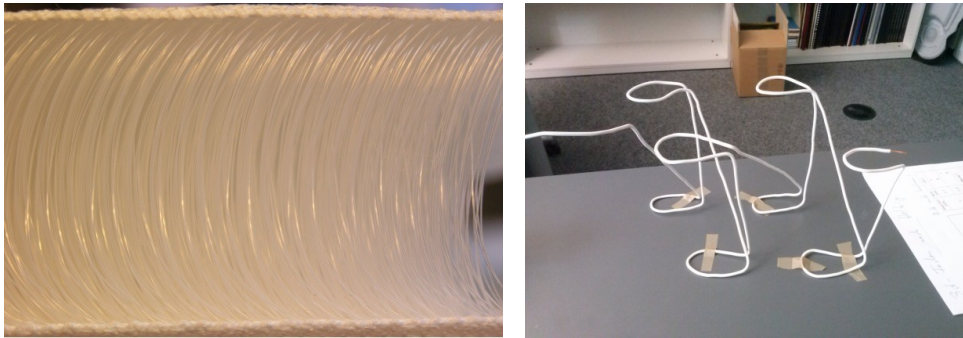

Figure 1. 50 mm spacer fabric, side view. Figure 2. Basic knitting element of Helbig structure.

2   EFFECTIVE ELASTIC PROPERTIES OF PERIODIC PLATES

We assume that this periodic structure is composed of thin beams. All in all when treating such a plate, we encounter several different small parameters. Firstly, we should mention that the period of the structure denoted by ε is very small, i.e. $\varepsilon \ll 1$. Besides that we also consider the thickness of the mentioned fibers $r \ll \varepsilon$. Our goal should then be to close the gap between the calculations of the homogeneous plate and the heterogeneous plate. The technique of our choice, which links this periodic structure to a homogeneous plate, is called homogenization, where we exploit the plate's periodicity. We will later homogenize the shells with this technique. The appropriate scaling, i.e. the choice of the small parameters, will be of particular importance. We start with the homogenization and dimension reduction of the shell and the computation of its effective stretching and bending properties. This will allow us to replace the heterogeneous porous plate by an equivalent homogeneous anisotropic plate.

3   Homogenization

First, the periodic 3D direct problem is introduced. Consider a bounded Lipschitz domain $\Omega^\varepsilon \subset (-L,L)^2 \times (-\varepsilon h/2,\ \varepsilon h/2)$, of the thickness $x_3 \in (-\varepsilon h/2,\ \varepsilon h/2)$. The domain is ε-periodic in $\mathbb{R}^2$ with periodically distributed holes. We study the following elliptic problem for linear elasticity in the domain as mentioned in [6, p.12].

$$
\begin{aligned}
-\nabla \cdot \left(a^\varepsilon(x) e(w^\varepsilon(x)) \right) &= f^\varepsilon(x) \text{ in } \Omega^\varepsilon, \\
w^\varepsilon &= 0 \text{ on } \partial\Omega_D^\varepsilon, \\
a^\varepsilon e(w^\varepsilon) \cdot n(x) &= 0 \text{ on } \partial\Omega_N^\varepsilon,
\end{aligned}
\tag{2.1}
$$

where $e(\bullet)$ is the symmetric part of the gradient and f^ε is the volume force. For further notes on this topic we refer to [6]. In general, we follow the Homogenization approach as discussed in [4]. In order to simplify the solution to equation 2.1 we study its asymptotic expansion as

$$
u_j^\varepsilon(x,t) = u_j\left(x,\frac{x}{\varepsilon},t\right) = u_j^0(x) + \varepsilon w_{pjq}(\xi)\frac{\partial u_q^0(x,\cdot)}{\partial x_p}\Big|_{\xi=\frac{x}{\varepsilon}} + O(\varepsilon^2),\ x \in \Omega
\tag{2.2}
$$

where $(w_{pq})_{3\times3\times3}$ lieves in Y, the periodicity cell. The limiting in-plane equation is

$$
\frac{\partial}{\partial x_i}\left(a_{ijkl}^{hom}\frac{\partial u_l^0}{\partial x_j} \right) = f_k(x_1,x_2),\quad k=1,2,\quad a_{ijkl}^{hom} = \varepsilon\frac{1}{|Y|}\int_{Y\backslash S} a_{iskt}\frac{\partial}{\partial y_s}(\boldsymbol{w}_{jlt} + \delta_{tl}y_i)dy
$$

$$
\frac{\partial}{\partial y_s}\left(a_{stkl}\frac{\partial}{\partial y_t}\left(\boldsymbol{w}_{ijl} + \delta_{jl}y_i \right) \right) = 0 \qquad \text{in} \quad Y\backslash S,
$$

$$
a_{3tkl}\frac{\partial}{\partial y_t}\left(\boldsymbol{w}_{ijl} + \delta_{jl}y_i \right) = 0 \qquad y_3 = \pm\frac{1}{2},
$$

The limiting equation of bending and equivalent homogeneous plate can then be determined as

$$
c_{1111}\frac{\partial^4 u_3^0}{\partial x_1^4} + c_{1122}\frac{\partial^4 u_3^0}{\partial x_1^2\partial x_2^2} + c_{2222}\frac{\partial^4 u_3^0}{\partial x_2^4} = f_3(x_1,x_2),\ (x_1,x_2) \in (-L,L)^2,
\tag{2.3}
$$

where the homogenized coefficients c_{ijkl}, according to [4, p.154-157], are calculated as

$$
c_{ijkl} = -\varepsilon^3\frac{1}{|Y|}\int_Y y_3\left(a_{jsit}\frac{\partial \boldsymbol{w}_{klt}^{(3)}}{\partial y_s} - a_{jkil}y_3 \right)dy,\quad i,j,k,l \in \{1,2\}
\tag{2.4}
$$

And the $u^{(3)}{}_{ij},\ i,j \in \{1,2\}$ are the Y-periodic solutions to the cell problems

$$
\frac{\partial}{\partial y_s}\left(a_{stkl_1}\frac{\partial \boldsymbol{w}_{ijl_1}^{(3)}}{\partial y_t} - a_{sikl_2}\delta_{jl_2}y_3 \right) = 0 \qquad \text{in } Y
$$

$$
a_{3tkl_1}\frac{\partial \boldsymbol{w}_{ijl_1}^{(3)}}{\partial y_t} - a_{3ikl_2}\delta_{jl_2}y_3 = 0 \qquad y_3 = \pm\frac{1}{2},
\tag{2.5}
$$

where the δ_{tl} are perturbations of the periodic conditions. Before we consider solving the cell-problems, we state a small remark about the bending stresses.

Remark. *The bending stresses can be computed from 2.5 as shown in [4] as*

$$\sigma_{i3}^{0\ bending}(x,y) = \frac{1}{|Y|} y_3 \left(a_{jsit} \frac{\partial w_{klt}^{(3)}}{\partial y_s} - a_{jkil} y_3 \right) \frac{\partial^2 u_3^0(x)}{\partial x_q^2} =: \frac{1}{|Y|} y_3 \sigma_{iq}^{cell}(y) \frac{\partial^2 u_3^0(x)}{\partial x_q^2} \qquad (2.6)$$

4   Dimension reduction

In the next step we want to account to the fact, that the solid pieces of the plate structures are beams. Therefore, we introduce a reduction of our periodic cell-problem to beam models and compute the effective properties. The computation of these have been presented earlier and we follow the techniques in [4], which have also been applied in [6]. We consider a one-dimensional geometry of a periodicity cell (a graph or fiber network) and take a node *n*. For one of its adjacent edges $e \in E(n)$ define $\gamma(e,n)$ to be directional vector of the edge pointing to *n*. Furthermore, let (g_1, g_2, g_3) be the global base and for each edge *e*, (l^e_1, l^e_2, l^e_3) defines the local base and C^e is the transformation matrix, such that $(l^e_1, l^e_2, l^e_3) = (g_1, g_2, g_3)\, C^e$. According to the homogenization technique the coefficients are obtained from cell-problems with periodic boundary conditions on the graph. The cell-problems that we look at are indexed by two numbers $i \in \{1,2,3\}$ and $j \in \{1,2,3\}$, such that $(i,j) \neq (3,3)$ and can be formulated as follows: find the periodic displacement fields $u_{ij} \in Y \to \mathbb{R}^{1\times 6}$, such that the auxiliary vector field $m_{ij} = u_{ij} + S_{ij}$, which was shifted by the unit perturbations, corresponding to the tension, shear, bending or torsion experiments, solves the following problem

at each edge e define $m_{ij}^e \in [0;l^e] \to \mathbb{R}^{1\times 4}$, $1 \leq i \leq 3$, $1 \leq j \leq 3$, $(i,j) \neq (3,3)$

$[m_{ij}^e]_1 \in H^1([0;l^e])$, $[m_{ij}^e]_2 \in H^2([0;l^e])$, $[m_{ij}^e]_3 \in H^2([0;l^e])$, $[m_{ij}^e]_4 \in H^1([0;l^e])$,

$m_{ij}^e \in \mathbb{R}^1 \to \mathbb{R}^{1\times 4}$, $1 \leq i \leq 3$, $1 \leq j \leq 3$, $(i,j) \neq (3,3)$

equilibrium conditions on edges hold:

$E^e A^e \frac{\partial^2}{\partial \chi^2} [m_{ij}^e]_1 = 0,$

$E^e I_2^e \frac{\partial^4}{\partial \chi^4} [m_{ij}^e]_2 = 0,$

$E^e I_3^e \frac{\partial^4}{\partial \chi^4} [m_{ij}^e]_3 = 0,$

$G^e M^e \frac{\partial^2}{\partial \chi^2} [m_{ij}^e]_4 = 0,$

force balance conditions in nodes hold:

$\sum_{e\in E(n)} E^e C^e \left(A^e \left([m_{ij}^e]_1\right)'_\chi \quad I_2^e \left([m_{ij}^e]_2\right)'''_\chi \quad I_3^e \left([m_{ij}^e]_3\right)'''_\chi \right)^T = 0,$

moment balance conditions in nodes hold:

$\sum_{e\in E(n)} C^e \left(G^e M^e \left([m_{ij}^e]_4\right)'_\chi \quad -E^e I_2^e \left([m_{ij}^e]_3\right)''_\chi \quad E^e I_3^e \left([m_{ij}^e]_2\right)''_\chi \right)^T = 0,$

periodic w.r.t. the periodic boundary conditions hold:

$[u_{ij}]_{1:3} \equiv C^e \left([u_{ij}]_{1:3} - S_{ij}\right)$ and $[u_{ij}]_{4:6} \equiv C^e \left(\begin{pmatrix} [m_{ij}^e]_4 \\ -\frac{\partial}{\partial\chi}[m_{ij}^e]_3 \\ \frac{\partial}{\partial\chi}[m_{ij}^e]_2 \end{pmatrix} - F(S_{ij}) \right)$

are periodic.

$$(2.7)$$

In this system we denote by χ the longitudinal component. The numerous constants that appear in the equation are the area of cross-section A^e, the area moments w.r.t. the second and third axis I^e_2, I^e_3 and the polar moment M^e of the element. For a beam with radius r, these are determined as $A^e = \pi r^2$, $I^e_2 = I^e_3 = \pi r^4/4$ and $M^e = \pi r^4/2$. The last two constants are the Young's modulus E^e and the shear moduli G^e of the element. The notation $[\bullet]_{i:j}$ means the i-th to j-th component of the vector. Anyway, we should specify how the perturbations S_{ij} for the cell-experiments look like. In general they are determined as

$$S_{11} = \begin{pmatrix} x_1 \\ 0 \\ 0 \end{pmatrix}, \quad S_{12} = \begin{pmatrix} 0 \\ x_1 \\ 0 \end{pmatrix}, \quad S_{21} = \begin{pmatrix} x_2 \\ 0 \\ 0 \end{pmatrix}, \quad S_{22} = \begin{pmatrix} 0 \\ x_2 \\ 0 \end{pmatrix},$$

$$S_{13} = \begin{pmatrix} -x_1 x_3 \\ 0 \\ 0 \end{pmatrix}, \quad S_{23} = \begin{pmatrix} -x_2 x_3 \\ 0 \\ 0 \end{pmatrix}, \quad S_{31} = \begin{pmatrix} 0 \\ -x_1 x_3 \\ 0 \end{pmatrix}, \quad S_{32} = \begin{pmatrix} 0 \\ -x_2 x_3 \\ 0 \end{pmatrix}. \quad (2.8)$$

The operator F denotes the transformation of the unit 3D-vectors into the 3 rotational degrees of freedom. They are based on the formulas of [1] defined as

$$F(S_{ij}) = \begin{pmatrix} \theta_1 \\ \theta_2 \\ \theta_3 \end{pmatrix}, \text{ where} \quad (2.9)$$

$$\theta_1 = \frac{4}{\pi r^4} \int_\omega \left[(z_3 l^e_3 + z_2 l^e_2) \times S_{ij}(z) \right] l^e_2 \, dz_3 \, dz_2, \quad (2.10)$$

$$\theta_2 = \frac{4}{\pi r^4} \int_\omega \left[(z_3 l^e_3 + z_2 l^e_2) \times S_{ij}(z) \right] l^e_1 \, dz_3 \, dz_2, \quad (2.11)$$

$$\theta_3 = \frac{2}{\pi r^4} \int_\omega \left[(z_3 l^e_3 + z_2 l^e_2) \times S_{ij}(z) \right] l^e_3 \, dz_3 \, dz_2, \quad (2.12)$$

with ω being the cross-section of the beam and $z = (z_1, z_2, z_3)$ in the local coordinate system, s.t.

$$z = (x - x_{ln}) C^e, \quad (2.13)$$

where x_{ln} denotes the left node in the global coordinate system. Given the solution for these cell experiments we are able to calculate the effective properties of the cell on a beam level. If we follow [4, chapter 5] on this topic, then the bending coefficients are calculated as

$$c_{iijj} = -\frac{1}{|Y|} \int_Y y_3 \sigma_{ij}(y) dy, \quad (2.14)$$

where $\sigma_{ij}(y)$ are the corresponding stresses, hence we need to introduce a stress interpolation regarding our beam model. With our cell experiments we obtain 3 spatial displacements components and 3 angular displacement components for every node, i.e. for a whole beam we have 12 degrees of freedom. In [2], an approach to achieve form this 12D a 4D field and finally a 3D field is shown. If we take a beam with nodes u and v and components

$$u = (u_1, u_2, u_3, \theta_{u1}, \theta_{u2}, \theta_{u3})^T, \quad (2.15)$$

$$v = (v_1, v_2, v_3, \theta_{v1}, \theta_{v2}, \theta_{v3})^T, \quad (2.16)$$

then the 4D field is obtained via a polynomial interpolation, as explained in [2, p.92], where we multiply our component vector with the interpolation matrix $R \in \mathbb{R}^{4 \times 12}$, such that

$$u^{4D} = R \begin{pmatrix} u \\ v \end{pmatrix}. \tag{2.17}$$

Given this 4D field, we can follow [3] to introduce it to a 3D field, where the components are given as

$$u_1 = u_1^{4D} - x_2 \frac{\partial u_2^{4D}}{\partial x_1} - x_3 \frac{\partial u_3^{4D}}{\partial x_1} + w \frac{\partial u_4^{4D}}{\partial x_1}, \tag{2.18}$$

$$u_2 = u_2^{4D} - x_3 u_4^{4D} - \nu x_2 \frac{\partial u_1^{4D}}{\partial x_1}, \tag{2.19}$$

$$u_3 = u_3^{4D} + x_2 u_4^{4D} - \nu x_3 \frac{\partial u_1^{4D}}{\partial x_1}. \tag{2.20}$$

The parameter ω is a warping constant. Such a 3D interpolation is necessary for visualization purposes. A higher order approximation may be obtained if desired. Anyway, [3] showed furthermore that using these interpolations and the initial 4D field we can calculate the stresses in connection to Hooke's law. Eventually, we get to the point, where we can calculate the local stress field as

$$\sigma^{loc}(x) = \begin{pmatrix} E\left(\frac{\partial u_1^{4D}}{\partial x_1} - x_2 \frac{\partial^2 u_2^{4D}}{\partial x_1^2} - x_3 \frac{\partial^2 u_3^{4D}}{\partial x_1^2} \right) & -\mu x_3 \frac{\partial u_4^{4D}}{\partial x_1} & \mu x_2 \frac{\partial u_4^{4D}}{\partial x_1} \\ -\mu x_3 \frac{\partial u_4^{4D}}{\partial x_1} & 0 & 0 \\ \mu x_2 \frac{\partial u_4^{4D}}{\partial x_1} & 0 & 0 \end{pmatrix}, \tag{2.21}$$

with μ being the second Lamé constant. Let us denote a beam in its local coordinate system by $z \in [-a_k, a_k] \times \omega_\varepsilon$. If we pass our beam and local stress field into global coordinates and plug it in formula 2.14, this yields

$$c_{iijj} = \frac{1}{|Y|} \sum_{k=0}^{\#\text{elem in } Y} \int_{[-a_k,a_k] \times \omega_\varepsilon} (y_{ln,3,k} + C_{13}^e z_1 + C_{23}^e z_2 + C_{33}^e z_3)(C^e \sigma^{loc}(z)(C^e)^T) dz. \tag{2.22}$$

Here we denote by $y_{ln,3,k}$ the third coordinate of the kth beam's left node in Y. The rest follows from integration. The limiting bending stresses however are provided by substituting this expression in 2.6 such that we obtain

$$\sigma_{i3}^{0\,bending}(x,z) = \frac{1}{|Y|}(y_{ln,3,k} + C_{13}^e z_1 + C_{23}^e z_2 + C_{33}^e z_3)(C^e \sigma^{loc}(z)(C^e)^T) \frac{\partial^2 u_3^0}{\partial x_i^2}, \tag{2.23}$$

where $x \in \Omega$ and $z \in [-a_k, a_k] \times \omega_\varepsilon$. This expression can also be written in the form

$$\sigma_{i3}^{0\,bending}(x,z) = B(z) \frac{\partial^2 u_3^0(x)}{\partial x_i^2}, \tag{2.24}$$

with the concentration factor $B(z)$ computed as

$$B(z) = \frac{1}{|Y|}((y_{ln,3,k} + C_{13}^e z_1)(C^e \Xi_1 (C^e)^T) + C_{23}^e z_2^2 (C^e \Xi_2 (C^e)^T) \tag{2.25}$$

$$+ C_{33}^e z_3^2 (C^e \Xi_3 (C^e)^T)), \tag{2.26}$$

and the Ξ_i given by

$$\Xi_1 = \begin{pmatrix} E\frac{\partial u_1^{4D}}{\partial z_1} & 0 & 0 \\ 0 & 0 & 0 \\ 0 & 0 & 0 \end{pmatrix}, \Xi_2 = \begin{pmatrix} E\frac{\partial^2 u_2^{4D}}{\partial z_1^2} & 0 & \mu\frac{\partial u_4^{4D}}{\partial z_1} \\ 0 & 0 & 0 \\ \mu\frac{\partial u_4^{4D}}{\partial z_1} & 0 & 0 \end{pmatrix}, \Xi_3 = \begin{pmatrix} -E\frac{\partial^2 u_3^{4D}}{\partial z_1^2} & -\mu\frac{\partial u_4^{4D}}{\partial z_1} & 0 \\ -\mu\frac{\partial u_4^{4D}}{\partial z_1} & 0 & 0 \\ 0 & 0 & 0 \end{pmatrix}.$$

$$(2.27)$$

5   MODELLING. ELASTIC PROPERTIES

The spacer fabrics were modelled using 1D-beam model, i.e. every thread of the actual model is represented as a union of straight 1D-segments (see Figure 4). Although this model is used for the sake of simplicity it actually represents the original material reasonably well, since the radius of the threads is small comparing to the length of the lines, i.e. the distance between horizontal layers. Since the model is one-dimensional it allows for fast and effective computation of effective elastic properties of the structure considered as a homogeneous material. Using the own software FiberFEM eight generated samples were simulated and effective properties were obtained. Table 1 contains the parameters of all tested samples, as well as the results of computer simulations. Used elastic properties of threads were provided by TU Dresden and are mentioned in the table below. The size of the periodicity cell was: width=1,875 mm., length=1,19 mm.

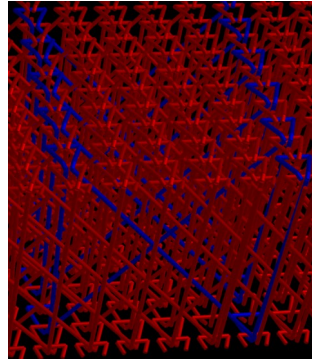| Fringe yarn	r=0,08 mm	E=8,0 GPa	nu=0,5
Connecter	r=0,05 mm	E=7,0 GPa	nu=0,5
Monofile (3D)	r=rmo (varied)	E=9,2 GPa	nu=0,5

Figure 4. Radius and elastic properties of threads. Structure of Sample 2.

	Parameters			In-plane properties		Bending properties	
	dist(mm)	diag(#)	radius(mm)	E1	E2	E1_bending	E2_bending
Sample 1	10	10	0.1	0.6693	0.1337	0.0383	0.0277
Sample 2	20	5	0.1	0.2930	0.1337	0.0206	0.0149
Sample 3	20	10	0.09	0.4223	0.1150	0.0188	0.0131
Sample 4	20	10	0.1	0.4861	0.1335	0.0206	0.0149
Sample 5	20	10	0.11	0.5530	0.1577	0.0226	0.0173
Sample 6	20	17	0.1	0.6457	0.1331	0.0206	0.0149
Sample 7	30	10	0.1	0.3818	0.1332	0.0141	0.0102
Sample 8	50	17	0.11	0.4531	0.1568	0.0095	0.0073
physical samples							

Table 1. Effective elastic properties of generated fabrics.

The results of the simulations show that the increase of the radius of the threads leads to the growth of Young's modulus. Similar effect is observed when parameter *diag* grows.

Another property of great interest is permeability of the material, i.e. the its ability to allow fluids to pass through. This property may vary provided that the material is compressed. Here a

big role plays another important advantage of the 1D model: it provides a fast and efficient way to simulate large deformations of the material. Using this feature the dependency between the level of compression of the material and its permeability was studied. 2% and 10% compression in vertical direction Z was applied to the samples 4 and 8, since they represent actual physical samples. The resulting deformed geometry is shown in Figure 5, as well as the local stress caused by deformation. The description and the results of flow simulation are discussed in the section below.
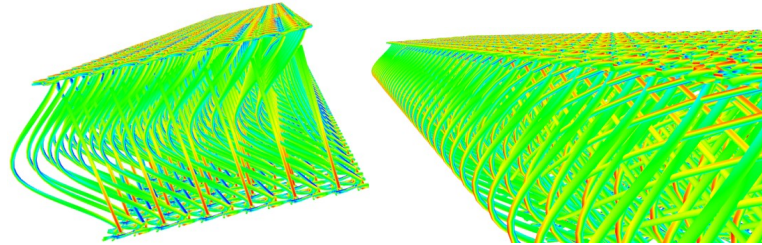

Figure 5. Local stresses in the fabric under compression.

6   PERMEABILITY OF DEFORMED AND UNDEFORMED MATERIAL

As it was mentioned before, permeability of the porous material describes its property to let fluids flow through it. Permeability depends on the inner geometry of the material, especially on the amount of pores. It does not depend on the type of fluid, so the obtained results are valid for any type of fluid, for example water, blood or even air.

The software called GeoDict provides an effective framework for flow simulation and for computing the permeability of the porous material. It uses voxel representation of material, so all 1D models generated before were converted into voxel formats. Computation only requires a small representative element, periodicity cell, which still contains enough information about the material. For flow simulation the pressure difference of 0.02 Pa was applied to all samples. The results are effective permeable properties, as well as the velocity and pressure fields (see Figure 6). Table 2 contains permeability for eight generated samples in three spatial dimensions X, Y and Z. Here direction Z is vertical direction from one horizontal layer to another, while X and Y denote two horizontal directions parallel to horizontal layers.
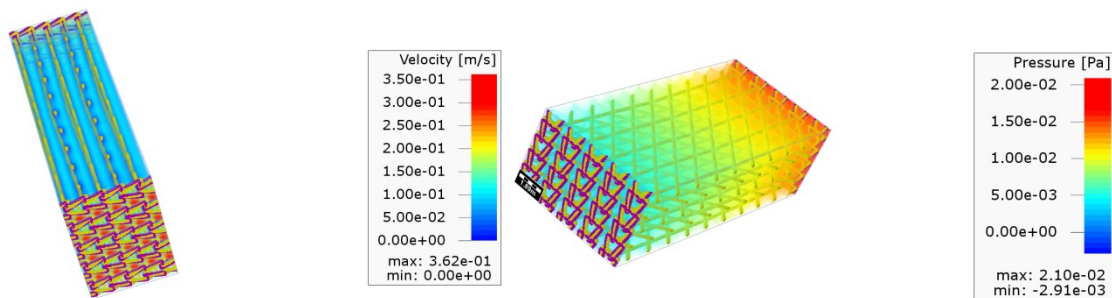

Figure 6. Examples of velocity and pressure visualization for Sample 4.

	Parameters				Permeability (mDarcy)		
	dist(mm)	diag(#)	radius(mm)	Solid part (%)	X-direction	Y-direction	Z-direction
Sample 1	10	10	0.1	6.04	6.547e+13	5.331e+13	3.528e+13
Sample 2	20	5	0.1	3.90	8.676e+13	1.115e+14	7.385e+13
Sample 3	20	10	0.09	3.56	9.245e+13	1.027e+14	6.942e+13
Sample 4	20	10	0.1	4.25	8.375e+13	9.370e+13	6.533e+13
Sample 5	20	10	0.11	5.00	7.655e+13	8.703e+13	6.140e+13
Sample 6	20	17	0.1	5.21	6.057e+13	7.942e+13	5.924e+13
Sample 7	30	10	0.1	3.70	8.819e+13	1.188e+14	8.925e+13
Sample 8	50	17	0.11	4.81	6.156e+13	1.176e+14	1.053e+14
physical samples							

Table 2. Permeability of different samples.

The results of the simulations show the predictable result that the increase of radius of the threads leads to the decrease of permeability since the part of the material occupied by solid body grows.

The relation between compression and permeability was investigated. To this end compression of 2% and 10% was applied in Z-direction. On resulting deformed geometry another flow simulation was conducted. The results for Sample 4 are presented in Table 3. The velocity fields in vertical and horizontal directions are visualized for undeformed geometry and 10% compressed geometry in Figure 7.

Sample 4		Permeability (mDarcy)		
Compression	Solid part (%)	X-direction	Y-direction	Z-direction
0%	4.25	8.375e+13	9.370e+13	6.533e+13
2%	4.29	9.423e+13	9.235e+13	6.631e+13
10%	4.99	6.719e+13	8.070e+13	5.749e+13

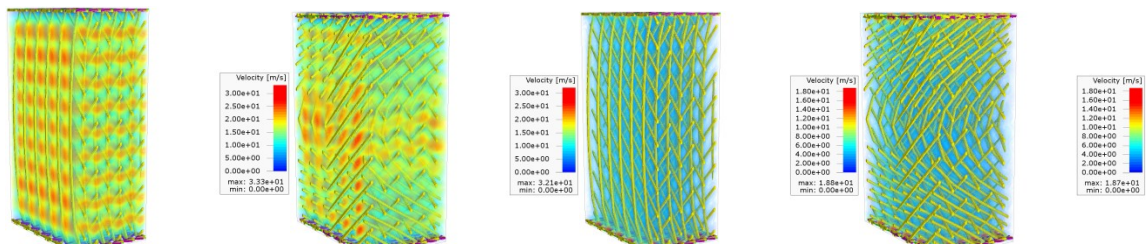Table 3. Permeability for compressed Sample 4.

Figure 7. Comparison of velocities in Y- and Z-directions in deformed and underformed configurations.

The results show that small compression leads to the growth of permeability. However further compression results in fast drop of permeability. The horizontal flow in deformed geometry is concentrated in the middle region, while in undeformed state it is distributed uniformly through the thickness.

REFERENCES

[1]   G. Griso. *Decompositions of displacements of thin structure*. J. Math. Pures Appl. 89, 199-223, 2008.

[2]   G.R. Liu, S.S. Quek. *The Finite Element Method, A Practical Course*. Butterworth-Heinemann, 2003.

[3]   L. Trabucho, J.M. Viaño. *Mathematical modelling of rods*. Hand book of Numerical Analysis, Vol. IV, 1996.

[4]   G. Panasenko. *Multi-scale modelling for structures and composites*. Springer Verlag, 2005.

[5]   F.U. Helbig. *Gestaltungsmerkmale und mechanishe Eigenschaften druckelastisher Abstandsgewirke*. http://d-nb.info/98092443X/34, 2006.

[6]   V. Shiryaev. *Modelling and design optimization of textile-like materials via homogenization and one-dimensional models of elasticity*. Technische Universität Kaiserslautern, 2015.

[7]   G. Griso, A. Migunova, J. Orlik. *Homogenization via unfolding in periodic layer wit contact*. Technische Universität Kaiserslautern, 2015.